metals

MDPI

Article

Electrochemical Synthesis of Polypyrrole and Polypyrrole-Indomethacin Coatings on NiCr Alloys Involving Deep Eutectic Solvents

Florentina Golgovici [1], Maria-Steliana Cârlan [2], Andreea-Gabriela Popescu [2] and Liana Anicai [3,*]

1 Department of General Chemistry, Faculty of Applied Chemistry and Materials Science, University Politehnica of Bucharest, Splaiul Independentei 313, 060042 Bucharest, Romania; florentina.golgovici@upb.ro
2 Faculty of Medical Engineering, University Politehnica of Bucharest, Splaiul Independentei 313, 060042 Bucharest, Romania; maya_dlr03@yahoo.com (M.-S.C.); andreeagabriela1710@yahoo.com (A.-G.P.)
3 Center of Surface Science and Nanotechnology, University Politehnica of Bucharest, Splaiul Independentei 313, 060042 Bucharest, Romania
* Correspondence: lanicai@itcnet.ro; Tel.: +40-723-685-319

Received: 30 June 2020; Accepted: 19 August 2020; Published: 21 August 2020

Abstract: There is an increased interest in the use of the deep eutectic solvents (DESs) as electrolytic media for electrochemical synthesis of conducting polymers, which could influence their characteristics. Moreover, the polypyrrole layers represent an attractive route for pharmaceutical drug release. The paper presents several experimental results regarding the electrodeposition of polypyrrole and of polypyrrole-indomethacin coatings on nickel-chromium NiCr alloy substrates widely used in dentistry, involving DES-based electrolytes, namely eutectic mixtures of choline chloride and malonic acid. This type of electrolyte also allowed an enhanced dissolution of indomethacin as compared to aqueous ones. The electropolymerization process has been investigated by cyclic voltammetry and chronoamperometry. The obtained indomethacin containing polymeric coatings have been thoroughly characterized involving scanning electron microscopy (SEM), Fourier transform infrared (FTIR) spectroscopy, contact angle measurements in simulated body fluid (SBF) and indomethacin release studies. Adherent and uniform polypyrrole-indomethacin layers have been obtained on NiCr alloy substrates. The release tests showed that the polypyrrole coatings containing indomethacin may deliver the drug molecules for longer periods of at least 17 days. The maximum released amount was around 99.6% suggesting these layers may act as an active reservoir for indomethacin. Kinetics analysis based on the Korsmeyer–Peppas model suggested the diffusion of the drug out of the polymer layer as the most probable mechanism governing the release.

Keywords: NiCr alloys; polypyrrole; deep eutectic solvents; indomethacin; drug delivery

1. Introduction

In recent years, due to the many uses of metals and alloys in dentistry and for economic reasons, the interest for non-precious dental alloys has increased. NiCr alloys are widely used in dental skeletal structures and orthopedic implants such as screws, pins, plates, crowns, bridge castings, inlays and denture bases [1–4]. Cr is the main alloying element facilitating a good corrosion performance due to the formation of a stable passive oxide layer [5–7]. The main concern regarding the use of NiCr alloys is the release of allergenic and toxic Ni^{2+} ions into the human body [8–12]. To circumvent this disadvantage, protective coatings also providing a suitable biocompatibility are largely investigated [13–17], including conducting polymers.

In the last decade the use of the electrochemically synthesized conducting polymers as coating layers has attracted an increased interest, due to their recognized biomedical compatibility [15,18]. Moreover, they can act as drug carriers as well, representing an alternative approach to conventional dosage forms. Usually, the film delivery systems are flexible sheets of polymeric matrices incorporating the therapeutic agent. They can be used for systemic or local action via several approaches including oral and transdermal delivery [19]. In particular, polypyrrole (PPy) layers have been extensively investigated and it has been shown they could represent an effective route to pharmaceutical drug release [14,15,18]. The electrochemical procedure is the most suitable to obtain PPy films on different substrates with a good adhesion and homogeneity, through a proper selection of the electrolyte composition and of the operating conditions. During the reversible change between PPy oxidized and reduced states the anions or cations are incorporated or released to maintain charge balance and these processes are linked with drug delivery.

The development of drug delivery systems sometimes suffers because of the poor solubility, permeability and stability of certain drugs. Especially the low solubility is a critical issue. Recently many studies showed an increased efficiency of the drug delivery systems when ionic liquids (ILs) are involved, which were found to provide an improved solubility/loading of poorly soluble drugs [20,21]. ILs are defined as "ionic materials in liquid state for temperatures lower than 100 °C" [22,23]. They are interesting chemical compounds with applications in a large range of domains including chemical and electrochemical synthesis procedures, due to their properties such as their ability to dissolve organic, inorganic and polymeric materials, non-flammability, high thermal and chemical stability, low vapor pressures and high ionic conductivity [22,24]. In this context, the related class of ILs known as "deep eutectic solvents" (DESs) has been shown to be more attractive in drug delivery systems mainly due to their lower toxicity as compared to classical ILs [21,25–27]. DESs are defined as eutectic mixtures of a quaternary ammonium salt such as choline chloride (2-hydroxy-ethyl-trimethyl ammonium chloride) with a hydrogen bond donor (HBD) species such as amides, glycols or carboxylic acids and have been reported for the first time by Abbott and his co-workers [28–30].

Indomethacin (1-(p-chlorobenzoyl)-5-methoxy-2-methylindole-3-acetic acid) belongs to the non-steroidal anti-inflammatory class of drugs, possessing analgesic, anti-febrile and antiaggregatory activity [31], with a proven efficiency for restorative procedures in deep cavities [32]. However, its poor solubility in water, ranging between 8.8 and 77 μg/mL [33] affects its applications [34,35]. It has been recently shown that the use of DESs may significantly increase the indomethacin solubility [36]. On the other hand, very few published works discussed the electrochemical synthesis of PPy involving various types of DESs [37,38]. Pigani et al. [38] reported the Py electropolymerization in choline chloride-ethylene glycol eutectic mixtures without the addition of any other species, using EQCM technique. The obtained PPy films using DESs were found to show comparable electroactivity to those grown in aqueous electrolytes. In addition, a higher degree of the film smoothness was noticed. Our group recently reported the PPy electrochemical synthesis involving choline chloride-malonic acid and choline chloride-oxalic acid eutectic mixtures (1:1 molar ratio) with additions of acetonitrile on Pt electrode [39].

Considering all discussed above, the present study aims to prepare adherent PPy layers on two types of NiCr alloys widely used in dentistry involving DES based electrolyte, able to incorporate indomethacin molecules as dopant which subsequently may be released in an aqueous environment. The electrochemical synthesis of PPy and of the indomethacin containing polymeric coatings on the two proposed NiCr alloys as substrate involving DESs, as well as their detailed characterization are reported. In addition, their protective characteristics and the release of the drug molecule in a simulated body fluid are presented and discussed. To the best of our knowledge this is the first investigation reporting the electropolymerization of pyrrole and of indomethacin doped PPy as adherent coatings on NiCr alloy metallic substrates involving DESs.

2. Materials and Methods

2.1. Materials

Two types of commercial NiCr alloys usually employed in dental medicine have been used as metallic substrates and their chemical composition is presented in Table 1. Niadur alloy (denoted ND) was supplied by DFS (Germany) and I-Bond alloy (denoted IB) was purchased from Interdent (Slovenia).

Table 1. Composition of the NiCr alloys.

Alloy Type	Composition/wt%							
	Cr	**Mo**	**Si**	**Fe**	**Co**	**Ce**	**Nb**	**Ni**
Niadur (ND)	24.5	10.3	1.7	1.5	-	-	-	balance
I-Bond (IB)	24.2	10.0	1.0	1.0	1.0	0.7	0.5	balance

Choline chloride ($HOC_2H_4N(CH_3)_3Cl$) (Aldrich, 99%), malonic acid ($CH_2(COOH)_2$ (Aldrich, 99%), acetonitrile (CH_3CN) (Aldrich, 99.8%) and indomethacin ($C_{19}H_{16}ClNO_4$) (Alfa Aesar, 99+%) were used as received. Pyrrole (C_4H_5N) (Py) (Aldrich, 98%) was distilled and stored under nitrogen until use.

As the investigated drug molecule, indomethacin (denoted Indo), has poor solubility in water, the electrochemical Py polymerization has been performed involving DES based electrolytes, consisting of choline chloride-malonic acid eutectic mixture (denoted ILM) (1:1 molar ratio) with additions (1:1 by volume) of acetonitrile (denoted ACN) to increase the conductivity. The monomer concentration was 0.5 mol/dm^3 (denoted M) Py. Choline chloride was mixed with malonic acid and heated at 75–85 °C with mild stirring until a homogeneous, clear liquid was formed. The as-prepared DES was cooled at room temperature (24 ± 2 °C) and ACN was added (1:1 by volume), followed by the addition of the corresponding amount of Py. Finally the Indo was introduced under continuous stirring, so that the final concentrations were in the range of 0.0125 M and 0.05 M.

2.2. Electropolymerisation of the PPy and of the PPy-Indomethacin Coatings onto NiCr Alloys

To get information on the electropolymerization of PPy and PPy-indomethacin coatings from DES based electrolytes, electrochemical techniques have been applied, including cyclic voltammetry and chronoamperometry, using an AutoLab 40 potentiostat/galvanostat (Radiometer Analytical SAS, Lyon, France). In these cases, a single-compartment glass cell was used, where NiCr alloy discs (1.4 cm diameter) with an exposed constant geometrical surface of 1.5 cm^2 acted as working electrodes. A high surface area platinum (Pt) plate was the counter electrode and a silver wire was the quasi-reference electrode [40]. Before each experiment the NiCr alloy working electrodes were mechanically polished using 1200-grit SiC abrasive paper, rinsed with deionized water, subjected to ultrasound cleaning for 10 min in acetone to remove any grease or impurities from the surface and air dried. After the polymer coating formation, the electrodes were abundantly rinsed with distilled water and air dried. All experiments were performed at room temperature, in stationary conditions. The voltammetric investigations were performed at scan rates between 10 and 50 mV s^{-1}. The formation of the PPy and PPy-indomethacin coatings was also investigated under potentiostatic conditions at different applied potentials for a constant polarization period of 600 s from different DES based electrolytes containing the monomer (Py), in the absence and in the presence of various Indo concentrations.

2.3. Characterization of the Electropolymerized Polypyrrole Coatings

The surface morphology of the prepared PPy and PPy-Indo coatings was examined by scanning electron microscopy (SEM) with a Quanta 650 FEG from Thermo Fisher Scientific (Hillsboro, OR, USA). To get information about their chemical composition the Fourier transform infrared (FTIR) spectrometry

(Jasco FT/IR 4000, Tokyo, Japan) was used. The spectra were collected from 4000 to 600 cm^{-1} with resolution of 4 cm^{-1} at 30 acquisitions per sample.

The surface wettability characteristics were determined by measurements of the contact angle in simulated body fluid (denoted SBF) at room temperature (24 ± 2 °C), using the preparation procedure as detailed in [41]. The involved SBF contains 7.996 g L^{-1} NaCl, 0.350 g L^{-1} $NaHCO_3$, 0.224 g L^{-1} KCl, 0.228 g L^{-1} $K_2HPO_4 \times 3H_2O$, 0.305 g L^{-1} $MgCl_2 \times 6H_2O$, 0.278 g L^{-1} $CaCl_2$, 0.071 g L^{-1} Na_2SO_4 and 6.057 g L^{-1} $(CH_2OH)_3CNH_2$ (tris(hydroxymethyl)aminomethane ACS as buffer). A CAM 100 compact contact angle meter was used and an average value of five measurements performed on five different areas of the specimens was considered.

The protective characteristics of the synthesized PPy and PPy-Indo layers were also assessed using SBF as electrolyte and the same three electrode cells. Potentiodynamic polarization curves at a sweeping rate of 5 $mV \cdot s^{-1}$ have been recorded against Ag/AgCl reference electrode and Pt mesh counter electrode. In these cases the polymer coatings were prepared under potentiostatic conditions, at a constant applied potential of 1.1 V vs. silver (Ag) wire and had a thickness d of 5.7 ±1 μm. It was determined by the gravimetric weight difference method using Equation (1), where m represents the mass of the deposited polymer in grams, ρ is the density of polypyrrole, taken as 1.5 g cm^{-3} and A is the surface area of the electrode, in cm^2:

$$d = \frac{m}{\rho \cdot A} \quad (1)$$

2.4. Drug Release Studies

The release of Indo molecules from the polymeric coatings were studied using optimized specimens of PPY-Indo coatings, which were placed in a 20 cm^3 SBF solution volume each. Prior to the drug release experiments, the polymer coatings were thoroughly washed with distilled water and dried. Periodic withdrawals of the solution containing the drug releasing specimens (three aliquots of 200 μL each) in combination with the use of a Perkin-Elmer UV-Vis spectrometer (Perkin-Elmer, Shelton, USA) allowed the construction of the drug release curves. Aliquots were analyzed by UV-Vis spectroscopy between 220 and 500 nm wavelengths. The values of the absorption band at 266 nm were considered and the average of three measurements was then used for the data analysis. A calibration straight line for indomethacin (correlation coefficient of 0.9986) was obtained using standards prepared with concentrations between 0 (blank) and 10 mg L^{-1}. The initial amount of the indomethacin in the polymer coating has been also determined employing the same analytical procedure.

2.5. Statistical Analysis

All performed measurements were checked in at least triplicate, in order to verify their reproducibility and to statistically evaluate their significance. Standard error was reported for all relevant data. To obtain more information on the morphological characteristics of the coatings, a statistical analysis was performed and the particle sizes were extracted from the high magnification SEM images by measuring approximately 50 individual particles for each sample. From the data represented in the form of histograms, the average particle sizes were calculated.

3. Results and Discussion

3.1. Electrochemical Preparation of PPy and of the PPy-Indo Coatings Using DES Based Electrolytes

Figure 1 presents the cyclic voltammograms recorded on the investigated NiCr alloys (IB and ND respectively) in ILM-ACN electrolyte in the absence of Py monomer.

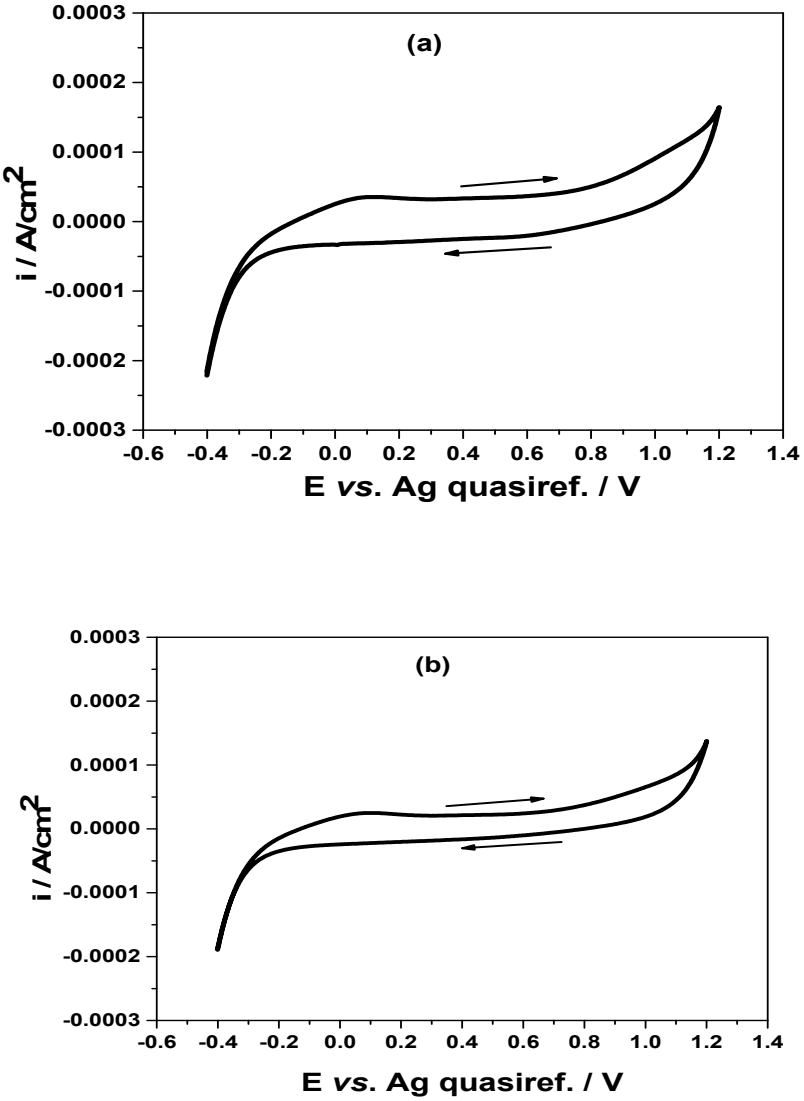

Figure 1. Cyclic voltammograms on NiCr alloys in ILM-ACN electrolyte: (**a**) IB alloy; (**b**) ND alloy. The scan rate was 10 mV s^{-1} and T = 25 °C.

Both figures show the presence of a current plateau followed by a continuous increase, as the electrode potential is displaced towards either more positive or negative values. The current values are relatively low, of 23 ÷ 35 μA cm^{-2} on anodic branch and of 16 ÷ 24 μA cm^{-2} on cathodic one. The onset of the anodic process is located at ca. +1.0 V, being assigned to the oxidation of chloride ion while the onset of cathodic one, at about –0.25 V is attributed to the electroreduction of hydrogen cations, a process in which hydrogen gas is formed [42].

Figure 2 illustrates examples of the recorded multicycle voltammograms (CVs) during PPy growth on IB (a) and ND (b) alloys from ILM-ACN electrolyte containing 0.5 M Py.

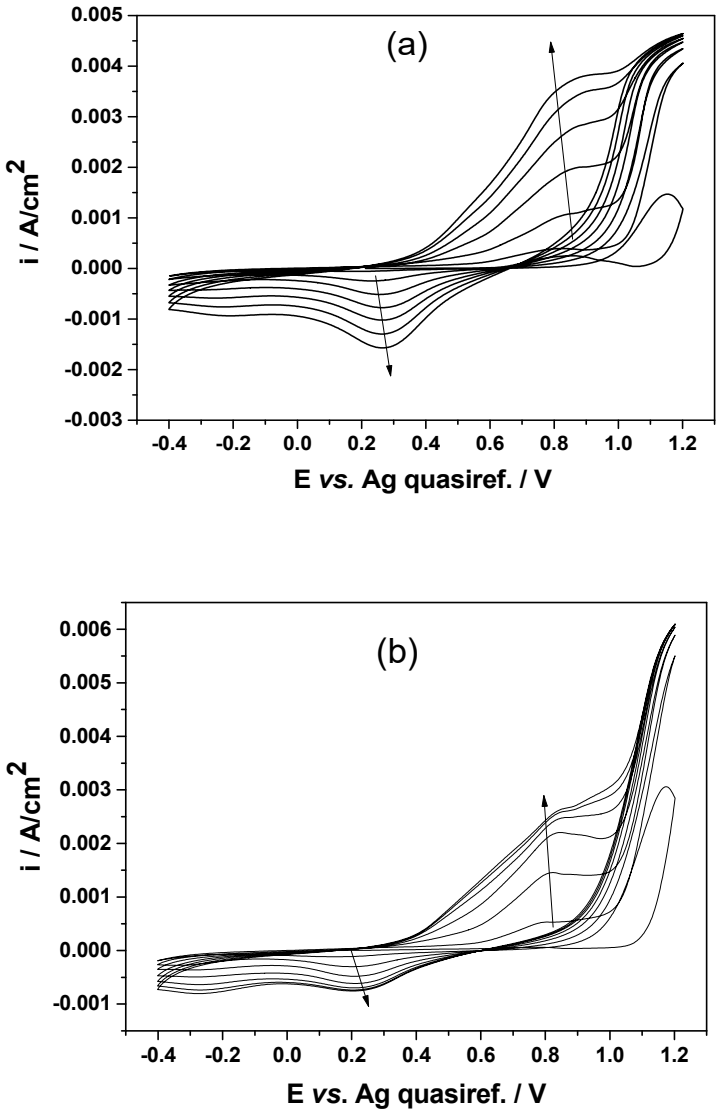

Figure 2. Cyclic voltammograms on IB (**a**) and ND (**b**) NiCr alloys during electrosynthesis of PPy from ILM-ACN electrolyte containing 0.5 M Py. The scan rate was 10 mV s^{-1} and T = 25 °C.

The first anodic scan presents a flattened anodic peak in the region 0.84–0.91 V/Ag on IB alloy (Figure 2a), respectively at around 0.83–0.86 V/Ag on ND alloy (Figure 2b). This indicates the oxidation of the pyrrole monomer, in other words, the onset of film growth producing the oligomer. If the scan is continued, a more clear anodic peak at about 1.14–1.16 V/Ag occurs which is attributed to oxidation process of Cl^- anions existing in the DES electrolyte. During repetitive cycling the current density increases with the number of potential cycling scans. This means a progressive increase in the electrical charge, the voltammograms displaying only the anodic plateaus at about 0.85–0.91 V/Ag, assigned to the further electropolymerization and PPy formation. As Garfias-Garcia et al. have shown [43], if the electropolymerization process continues, the potential required to polymerize may become less positive than that corresponding to the monomer oxidation.

Correspondingly, the peaks at 0.23 ÷ 0.27 V/Ag for the IB alloy, respectively at 0.21 ÷ 0.22 V/Ag for the ND alloy identified on the cathodic branch of the CVs are assigned to the reduction process. This reduction peak increase could be associated with the expulsion of a fraction of Cl^- species originated from the DES (deintercalation of Cl^- anions in order to maintain charge neutrality) from the polymer film due to its reduction from the oxidized to the neutral state, in agreement with [44].

The significant increase in current in the whole potential range with increasing the number of cycles indicates the growth of the PPy layer on both investigated NiCr alloys.

According to Figure 2, a slightly higher polymerization rate was noticed on the IB type alloy, materialized by current density values around 3.8 mA cm^{-2} after six cycles as compared to about 2.66 mA cm^{-2} in the case of the ND type alloy after the same number of cycles. This phenomenon could be related to the slight difference in the value of the potential required to initiate the Py oxidation on the two investigated NiCr alloys, which may suggest the formation of different oligomeric species of Py depending on the alloy type (IB or ND type) [43] which further influence the overall growth kinetics.

After electropolymerization, both types of NiCr alloy were entirely covered by a black, uniform and adherent PPy layer.

The PPy films were also synthesized onto the IB and ND alloys under potentiostatic conditions. Figure 3 illustrates typical current versus time curves obtained for the potentiostatic synthesis of PPy on the two investigated NiCr alloys as substrates at different applied potentials (E_f) using ILM-ACN electrolyte.

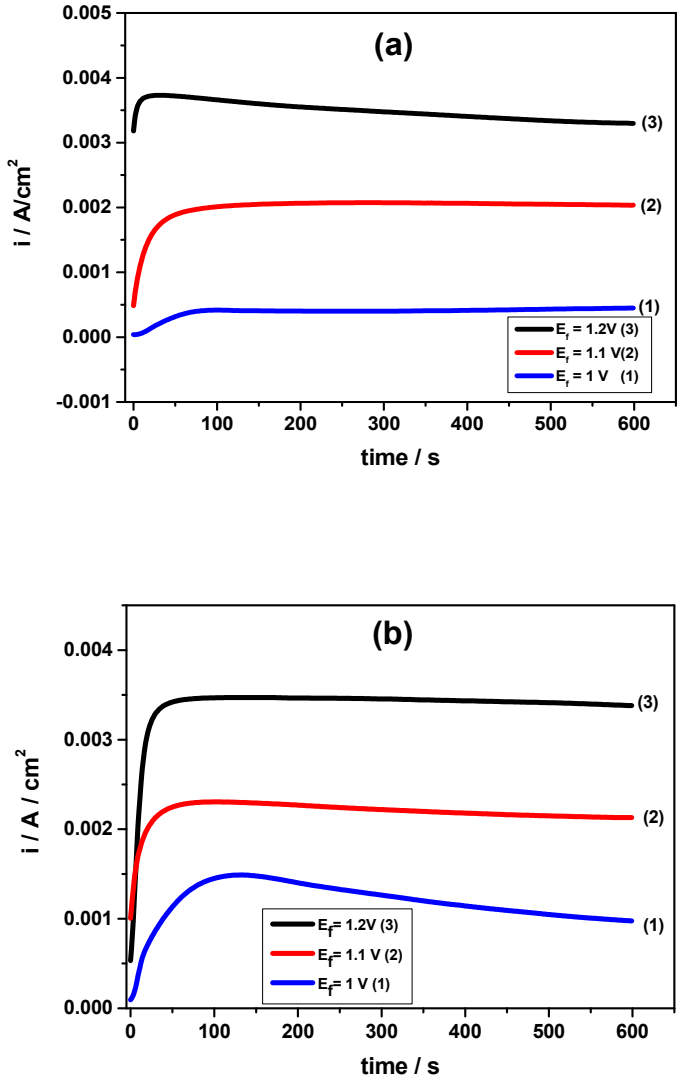

Figure 3. Current–time plots recorded at different constant applied potentials for electrosynthesis of PPy from ILM-ACN electrolyte containing 0.5 M Py on IB (**a**) and ND (**b**) NiCr alloys.

The curves can be divided in two periods: (1) an increased anodic current, corresponding to the onset of PPy electropolymerization and (2) a current stabilizing in time. The first part shows an increase

of the anodic current known as the induction period [45] due to the nucleation and growth of the polymer; in some cases the current reaches a maximum. Then the current slightly decays or remains constant attaining a near steady-state value. As illustrated in Figure 3, the shape was found to be dependent on the applied potential. As expected, a potential increase from 1 to 1.2 V (vs. Ag quasiref.) produces an increase in the charge required for anodic polymerization, in agreement with [45,46]. The recorded current-time plots at constant applied potentials showed a relatively similar behavior for the two investigated alloys.

Examples of the recorded CVs during Py electrochemical polymerization in ILM-ACN electrolyte in the presence of 0.0175 M Indo are displayed in Figure 4.

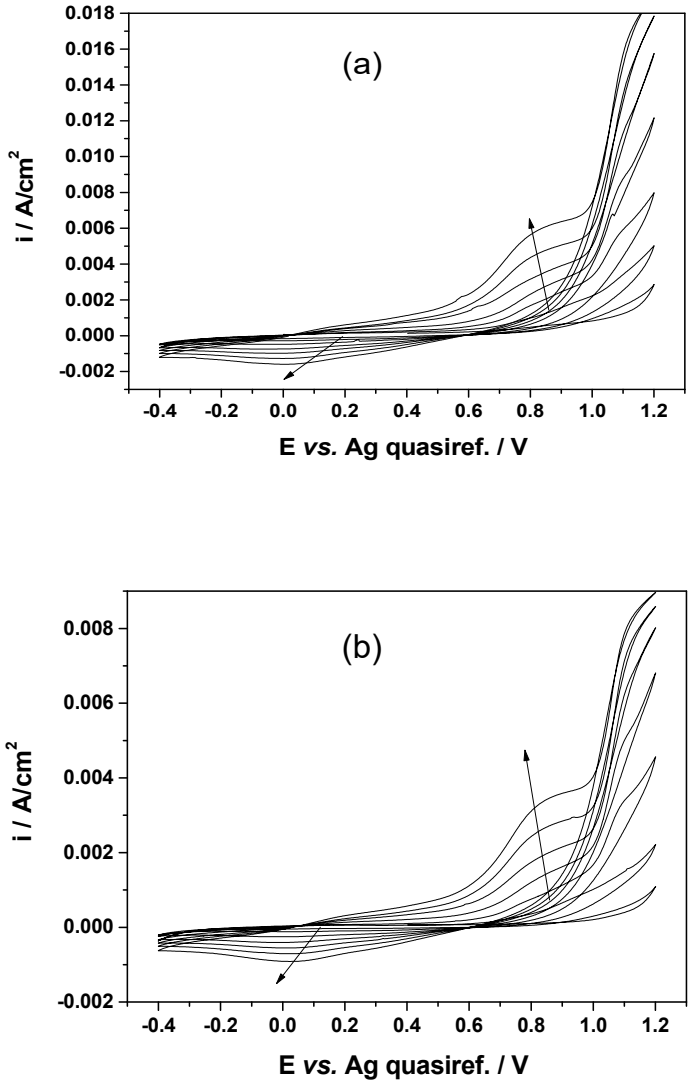

Figure 4. Cyclic voltammograms on IB (**a**) and ND (**b**) NiCr alloys during electrosynthesis of PPy-Indo from ILM-ACN electrolyte containing 0.5 M Py and 0.0175 M Indo. (scan rate of 10 mV s^{-1} and 25 °C).

The shapes of the voltammograms are similar to those recorded in the absence of Indo, for both investigated NiCr alloys. In addition, higher anodic currents are noticed by comparing CV curves from Figures 2 and 4, suggesting the incorporation of Indo charged species within the PPy matrix which increases the required charge for polymerization. It is known [47,48] that the Indo molecule contains several hydrophilic groups, including carboxylic group, –COOH, amide group, –CONH–, and methoxyl group, $–OCH_3$ that can participate in different hydrogen bonding interactions leading to

formation of cyclic aggregates such as dimers and linear chains. They may be either hydrogen bond (HB) donors, acceptors or both.

Based on several experiments at different deposition periods and applied potentials associated with the quality of the prepared films, the optimum parameters for PPy growth on IB and ND type alloys with a high degree of reproducibility were found to be 600 s and 1.1 V (vs. Ag quasiref.), respectively.

Therefore, the further electrochemical synthesis of the PPy-Indo coatings was performed under potentiostatic conditions at an applied potential of 1.1 V for 600 s involving ILM-ACN electrolyte containing 0.5 M Py and different concentrations of Indo in the range of 0.0125–0.05 M.

Figure 5 presents examples of the recorded charge–time plots for the studied NiCr alloys during potentiostatic PPy polymerization in the absence and in the presence of Indo dissolved in ILM-ACN electrolyte containing 0.5 M Py.

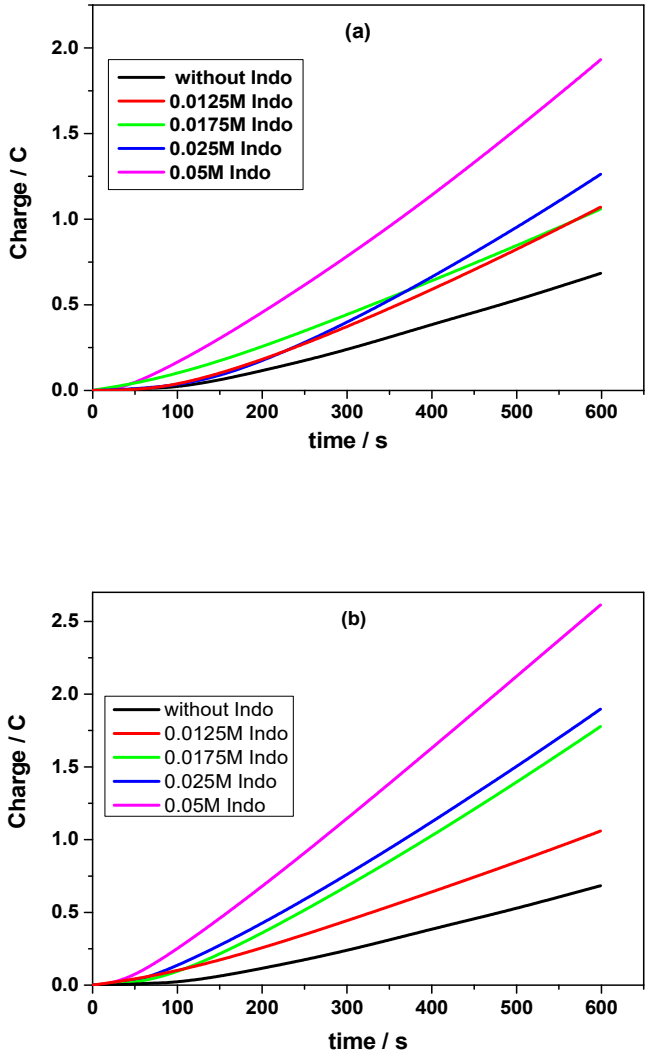

Figure 5. Charge–time plots during electrosynthesis of PPy and PPy-Indo at a constant potential of 1.1 V/Ag for 600 s on IB (**a**) and ND (**b**) NiCr alloys from ILM-ACN electrolyte containing 0.5 M Py in the absence and in the presence of various Indo concentrations.

As evident from Figure 5, an increase in the Indo concentration produces an increase of the polymerization charge, regardless of the type of NiCr alloy substrate, thus confirming the voltammetric comparison of Figure 2 (electrolyte without Indo) and Figure 4 (with 0.0175 M Indo).

The polymerization charge obtained for different Indo concentrations in the ILM-ACN based electrolytes is summarized in Table 2.

Table 2. Polymerization charge for different Indo concentrations in ILM-ACN based electrolytes.

Alloy Type	Electrosynthesis Electrolyte	Applied Potential During 600 s (V vs. Ag)	Polymerization Charge/C cm^{-2}
IB	0.5M Py	1.1	0.844
	0.5M Py +0.0125M Indo		0.864
	0.5M Py +0.0175M Indo		0.78
	0.5M Py +0.025M Indo		1.068
	0.5M Py +0.05M Indo		1.416
ND	0.5M Py	1.1	0.564
	0.5M Py +0.0125M Indo		0.78
	0.5M Py +0.0175M Indo		1.404
	0.5M Py +0.025M Indo		1.452
	0.5M Py +0.05M Indo		1.932

Usually, from the gradient of the charge–time plot, the rate of polymer deposition can be estimated and any deviation from the linear trend would suggest a loss in the conductivity of the deposited polymer [46]. Therefore, rates of electrochemical polymerization were calculated for the investigated Indo doped PPy coatings, ranging between 2.16 and 3.54 mC s^{-1} (1.44–2.36 mC cm^{-2} s^{-1}) and 2.0–4.83 mC s^{-1} (1.3–3.22 mC cm^{-2} s^{-1}) for IB and ND substrates, respectively. It should be noticed that the PPy-Indo coating formation on ND alloy is slightly faster than on IB type. For both cases charge–time linear plots have been recorded, giving a constant rate of electropolymerization, with no evidence of any decrease in the conductivity of the deposited polymer [46,47].

3.2. Characterization of Indo Doped PPy Coatings

In order to get information on the morphology of the PPy-Indo coatings formed on the involved NiCr alloys under potentiostatic control in ILM-ACN based electrolyte, SEM microscopy has been applied. Figure 6 presents examples of the SEM micrographs of the electrochemically synthesized polymeric layers on the two investigated metallic substrates.

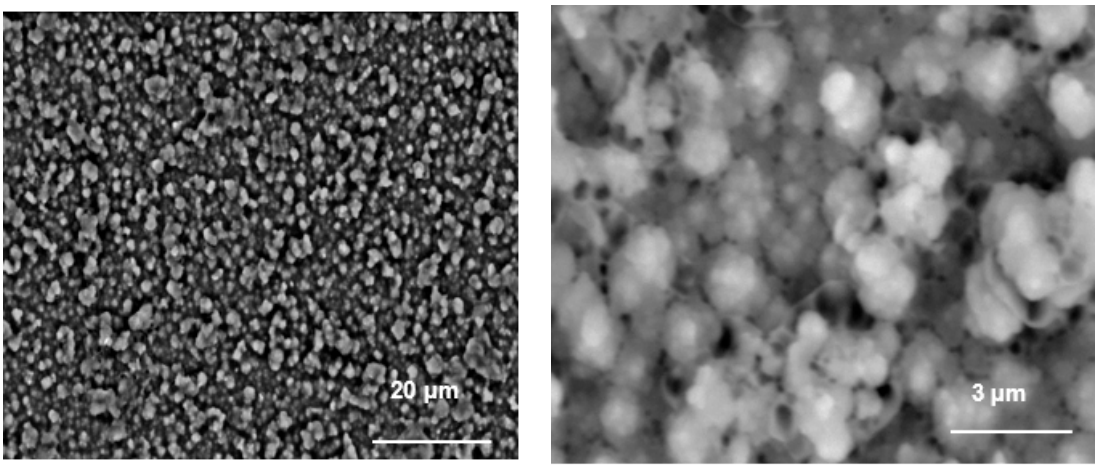

(**a**)

Figure 6. *Cont.*

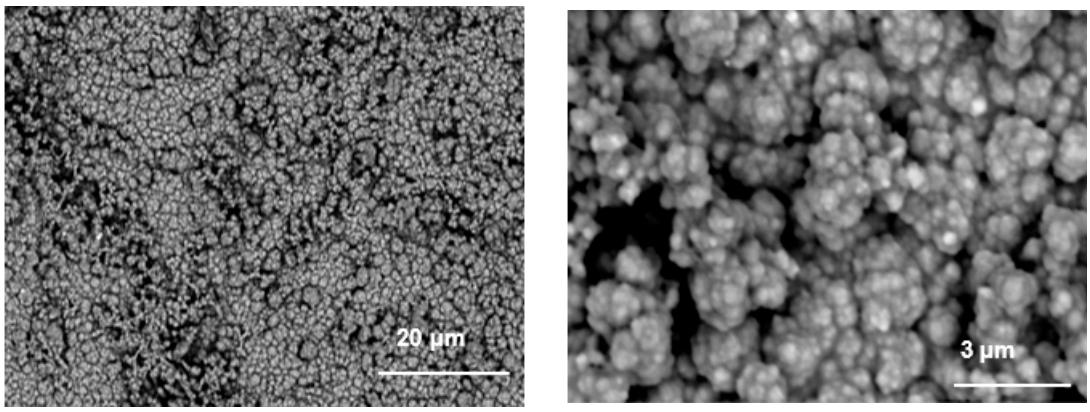

(**b**)

Figure 6. SEM micrographs at different magnifications for PPy-Indo coatings formed on: (**a**) IB and (**b**) ND alloy substrates from ILM-ACN electrolyte containing 0.5 M Py and 0.0175 M Indo at a constant applied potential of 1.1 V/Ag for 600 s.

The synthesized PPy-Indo polymer films show a rather granular surface morphology for both involved NiCr alloy types, quite consistent with previous findings in [39]. The average particle size was extracted from the high magnification SEM images by measuring approximately 50 individual particles for each sample. From the data represented in the form of histograms (not shown here) the highest number of particles was found to be within 160–220 nm range for the ND substrate and within 180–320 nm range for the IB substrate, respectively. The mean particle size was calculated as 200 ± 25 nm for the ND alloy and as 261 ±54 nm for the IB one. A slight porosity of the film is also observed, somewhat more pronounced for the IB metallic substrate. In addition, the SEM micrographs suggest that the IB alloy facilitates the formation of a more ordered and homogeneous layer as compared to the ND one. Moreover, from the recorded micrographs it is evident that there are no insoluble precipitates of the drug molecules on the surface.

The electrochemically synthesized PPy and PPy-Indo films have been qualitatively analyzed by FTIR spectroscopy, as exemplified in Figure 7.

The main peaks of indomethacin can be observed on FTIR spectra at 2900 cm^{-1} corresponding to Ar–H stretching vibration in aromatics (Ar), 2860 cm^{-1} associated with C–H stretch and 1740 cm^{-1} which is assigned to the C=O and C–O stretches. Moreover, the peak at 1468 cm^{-1} corresponds to O–CH_3 deformation and the peaks in the region of 708 cm^{-1} correspond to the presence of aromatic ring of indomethacin, as illustrated in Figure 7d,e [49,50]. A broad shoulder better evidenced in Figure 7b,c in the region 3400–3200 cm^{-1} may be assigned to the presence of N–H stretching vibrations of pyrrole ring [51,52]. The peak at 1566 cm^{-1} is attributed mainly to the intercycle C–C stretching vibration in PPy and the band centered at 1163 cm^{-1} can be associated with C–N stretch while the peak at 957 cm^{-1} is due to ring stretch from pyrrole [53,54]. All these peaks indicate the presence of indomethacin in the polypyrrole structure.

Contact angle, defined as the angle formed at the intersection of the liquid and the solid interface, represents a relative measure of the surface energy of a material. Usually, contact angle analysis may provide valuable information about hydrophilicity and the hydrophobicity nature of the material's surface. Therefore, the SBF contact angle was examined to get information on the wettability of the surface after each modification, which usually is governed by the chemical composition and surface morphology. Contact angles between 0° and 90° are characteristic to hydrophilic surfaces, while values higher than 90° indicate hydrophobic characteristics [55,56]. As illustrated in Figure 8, the bare NiCr alloys showed significant hydrophobicity, more pronounced for ND alloy. The presence of the electropolymerized PPy layer produced a significant decrease around 29° and 38° for both the IB and the ND alloys, respectively.

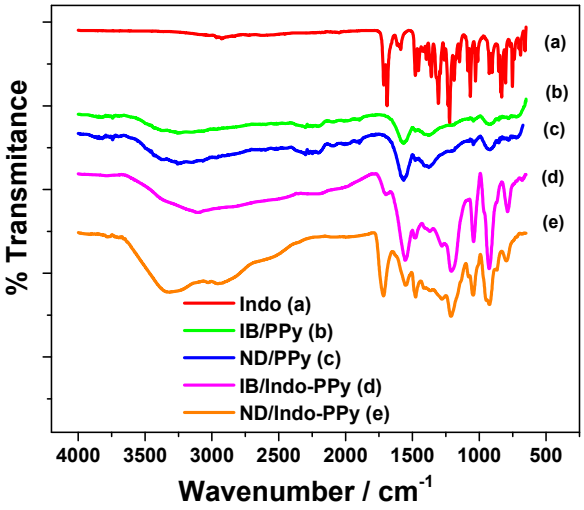

Figure 7. Representative FTIR spectra of electrochemically synthesized PPy (b,c) and PPy-Indo (d,e) coatings on IB and ND alloy substrates from ILM-ACN based electrolyte containing 0.5 M Py and 0.0175 M Indo. The spectrum of pure Indo (a) is also shown.

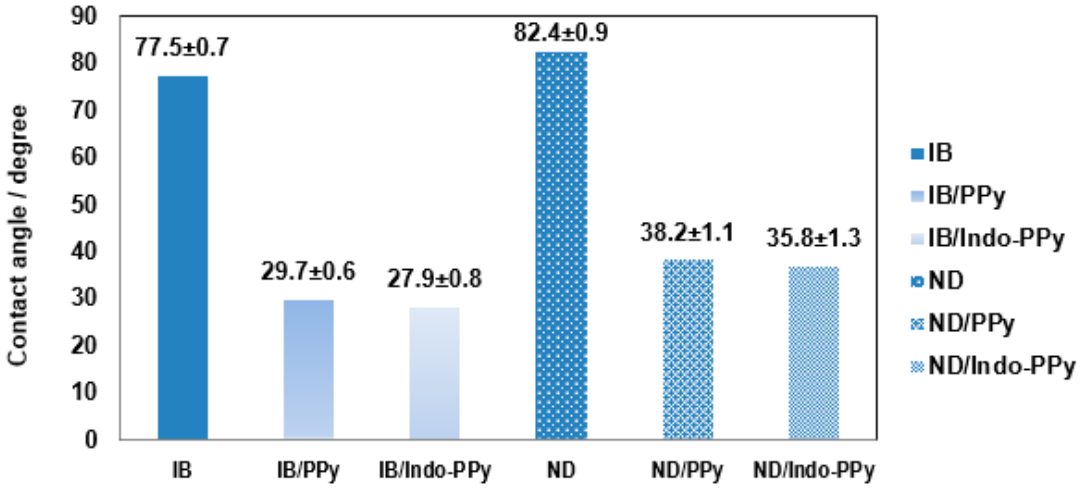

Figure 8. Contact angles of the bare NiCr investigated alloys, of the electrochemically synthesized PPy and PPy-Indo coatings.

Moreover, the doping with Indo also contributed to a decrease of the contact angle value, suggesting an improvement of the hydrophilic characteristics. This behavior could be related to the slightly porous morphology of the Indo doped PPy coatings, more pronounced in the case of IB alloy as metallic substrate. It is worth mentioning here that the SBF contact angle measurements evidenced quite similar values, regardless of the value of Indo concentration in the DES based electrolyte during electropolymerization.

The protective characteristics of the Indo doped PPy coatings on both the IB and the ND alloy substrates have been assessed in SBF as electrolyte, using linear sweep voltammetry. Figure 9 comparatively presents typical potentiodynamic polarization curves for PPy and Indo doped PPy coatings electrosynthesized from ILM-ACN based electrolyte on the two involved NiCr alloys having a constant thickness of 5.7 ± 1 μm.

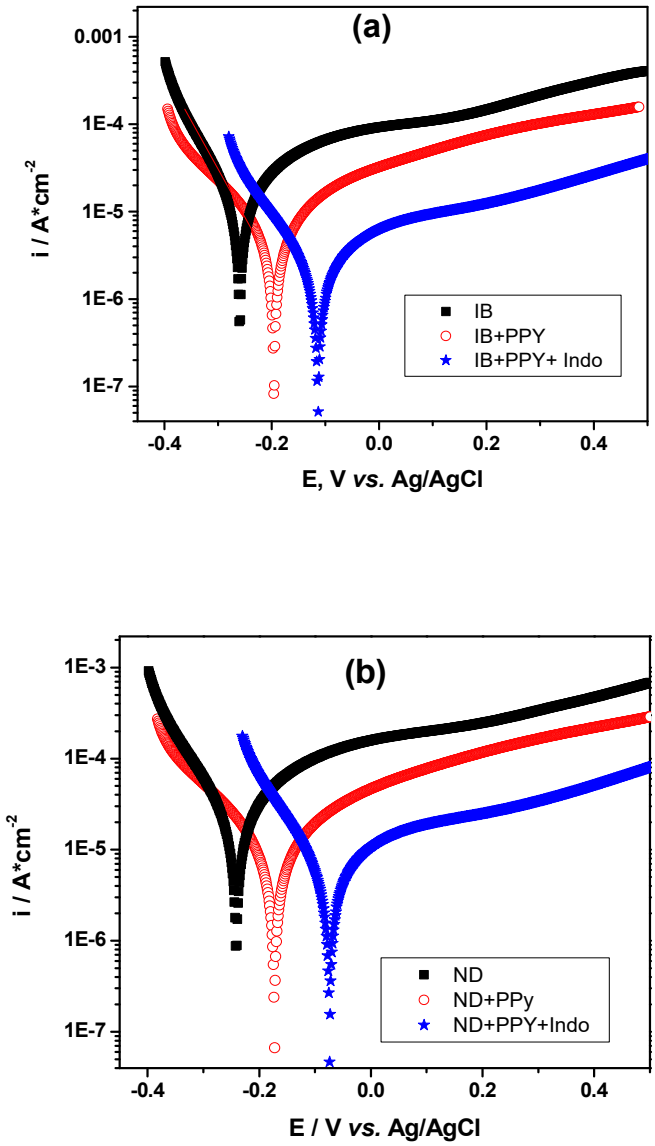

Figure 9. Polarization curves in semilogarithmic coordinates for PPy and PPy-Indo films formed at constant applied potential of 1.1 V/Ag on: (**a**) IB and (**b**) ND alloy substrates from ILM-ACN electrolyte containing 0.5 M Py and 0.0175 M Indo. Curves were recorded in SBF at 25 °C, scan rate 5 mV $s^{-1.}$

As the polarization measurements were performed with solution in contact with the atmosphere, dissolved oxygen molecules will normally be present and the cathodic currents recorded in the presented potential region can be attributed to the reduction of oxygen dissolved in the solution [57,58]. Analyzing the anodic part of the polarization curves, it is seen that the uncoated IB and ND alloys show a passive region up to ~0.1 ÷ 0.2 V vs. Ag/AgCl, followed by an increase of the current as the potential is shifted towards more positive values. It is obvious that the PPy and PPy-Indo coated electrodes also present passive regions, slightly displaced positively as compared to the uncoated alloys. In addition, the values of the corrosion potential E_{corr} of PPy and PPy-Indo layers are about 100–150 mV more positive than those of the uncoated alloys.

The values of the corrosion current density, i_{corr} and corrosion potential, E_{corr} (determined by Tafel extrapolation of both cathodic and anodic polarization curves) as well as values of the polarization resistance, R_p (calculated from the Stern–Geary equation) [59] are listed in Table 3. Corrosion rates, CR, were also obtained from these curves.

Usually, the polarization resistance R_p is representative for the degree of protection at the surface. When higher values of the R_p are noticed, lower i_{corr} may be expected. Therefore regarding the values presented in Table 3, it is obvious that the PPy-Indo layers exhibit better corrosion protection as compared to the PPy ones, for both investigated metallic substrates. As illustrated in Figure 9, the corrosion protection effect of PPy and PPy-Indo coatings is more related to the inhibition of anodic reaction.

Table 3. Values of corrosion parameters resulted from polarization curves in SBF for bare NiCr alloys, PPy and PPy-Indo coatings.

Alloy Type	Coating Type	E_{corr} /V vs.Ag/AgCl	i_{corr}/μA cm^2	CR/mm/year	R_p/Ω
IB	-	−0.260	11.82	0.143	2760
	IB-PPy	−0.208	4.18	0.051	7252
	IB-Ppy-Indo	−0.118	1.68	0.020	17,086
ND	-	−0.250	19.85	0.241	1345
	ND-PPy	−0.180	7.47	0.091	3820
	ND-Ppy-Indo	−0.078	4.65	0.056	11,562

3.3. Indomethacin Release from the Polypyrrole Matrix

The release of indomethacin from the polymer films was assessed by immersing the drug loaded specimens in the SBF at room temperature. The UV-Vis spectrum of indomethacin recorded in SBF between 220 and 500 nm is presented in Figure 10a, showing maximum absorption bands at 266 nm, 321 nm and 203 nm. The calibration curve illustrated in Figure 10b has been obtained for the highest absorption band at 266 nm. A good linearity has been noticed up to about 0.01 g L^{-1} (27.9 μM) of indomethacin in SBF, so that this medium could be considered appropriate for the release of the drug from the PPy matrix.

The PPy-Indo coatings employed in the release experiments were loaded with various amounts of Indo, depending on its concentration during electrochemical polymerization, as it follows: (i) 67.9 μg (0.0125 M Indo); (ii) 110.9 μg (0.0175 M Indo); (iii) 153.8 μg (0.025 M Indo) and (iv) 193.1 μg (0.05 M Indo).

Figures 11 and 12 show the release profiles of indomethacin from the doped conducting polymer coatings electrosynthesized on the IB and the ND metallic substrates, respectively, from ILM-ACN based electrolyte containing 0.5 M Py and various Indo concentrations. The cumulative drug release, denoted R, represents the fraction (percentage) of the active species released at time t in SBF medium, calculated as $R\% = 100 \times q/q_o$, where q_o represents the initial amount of the Indo in the coating and q is the released drug amount at time t.

As illustrated in Figure 11, an initial burst release effect up to about 30% during the first 12–15 h may be noticed for the PPy-Indo coatings on the IB substrate, followed by a prolonged release phase for the next 200–250 h and then a relatively constant release profile up to 400 h.

The doped conducting polymer coatings on ND substrate as presented in Figure 12 show an initial burst release of about 18% during the first 15 h, followed by a continuous prolonged release phase for the next 500–550 h.

According to the drug release profile, the electrochemically synthesized PPy-Indo coatings involving ILM-ACN based electrolytes have the potential to deliver indomethacin for longer periods of at least 17 days. The cumulative indomethacin released fraction is in the range of 98.7–99.6% after 408 h and between 95.7–99.6% after 600 h for the PPy-Indo coatings on the IB substrate and the ND one, respectively. This evolution suggests a faster release of the drug in the case of the doped conducting polymer coatings electrosynthesized on IB. Generally, the morphological characteristics of the films may influence the diffusion of the active compounds to the solution [60]. Therefore, the slightly higher porosity of the PPy-Indo layers on IB as it was shown in Figure 6a may support this faster release behavior.

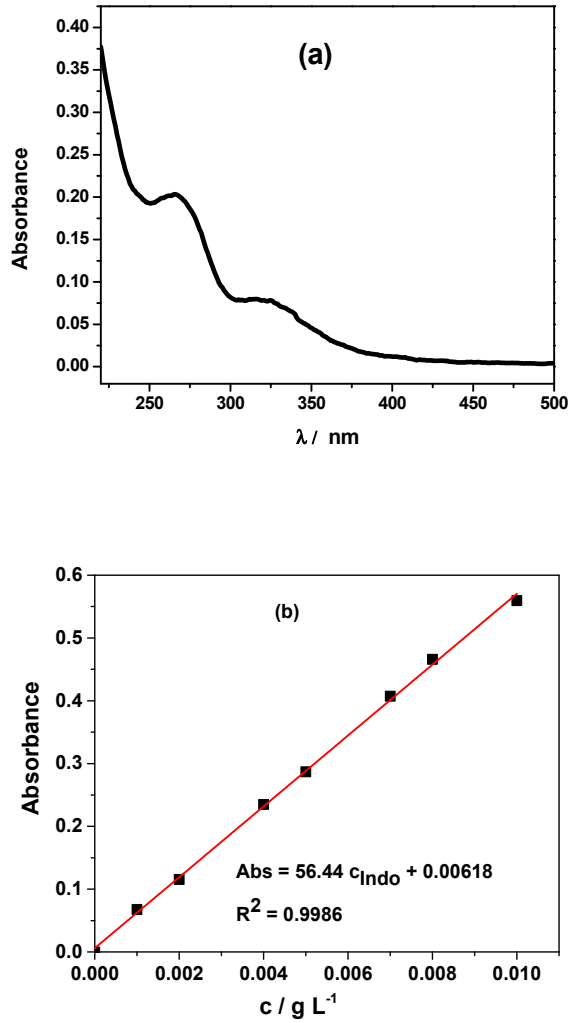

Figure 10. (**a**) UV-visible spectrum recorded for 0.01 g L^{-1} (27.9 μM) indomethacin dissolved in SBF; (**b**) calibration curve recorded in SBF for indomethacin (n = 3).

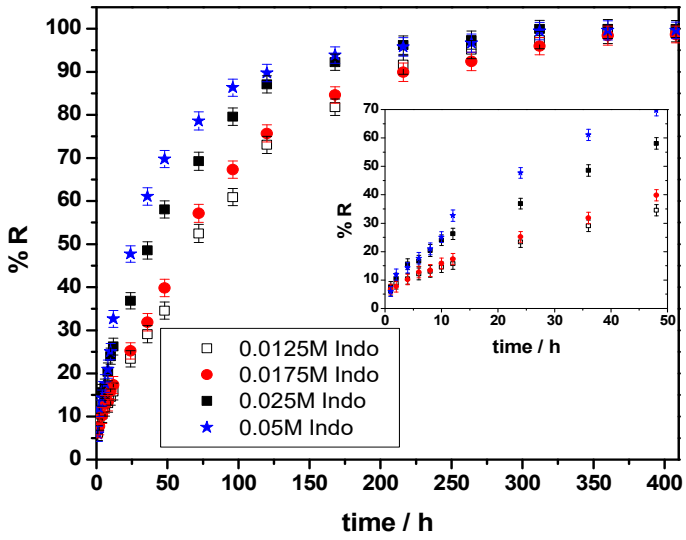

Figure 11. Indomethacin release profiles from the PPy-Indo coatings electrosynthesized on IB from ILM-ACN based electrolyte containing 0.5 M Py and various Indo concentrations. Inset: burst drug release.

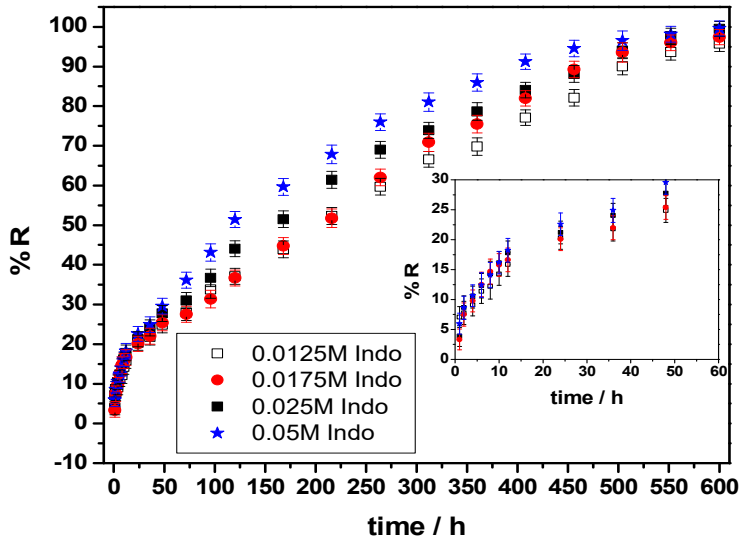

Figure 12. Indomethacin release profiles from the PPy-Indo coatings electrosynthesized on ND from ILM-ACN based electrolyte containing 0.5 M Py and various Indo concentrations. Inset: burst drug release.

The mathematical modeling of the indomethacin release from the PPy coatings can provide more information on the mechanism governing the release.

Most of the empirical and semi-empirical mathematical models that have been developed in order to kinetically study the release of drugs have been derived from Fick's law of diffusion [61–63]. The Korsmeyer–Peppas model, also known as the power law model is based on a simple semi-empirical equation frequently involved to describe the release kinetics in pharmaceutical research [61,63,64]. This equation is expressed as:

$$R = k\, t^n \quad (2)$$

where *R* is the cumulative drug release fraction at time t, k is kinetic constant also incorporating structural and geometric characteristics of the drug/polymer system and n represents the diffusional exponent characterizing the mechanism of the drug release [63,64]. The Korsmeyer–Peppas model may be seen as a decision parameter to identify drug transport mechanisms where n is used to differentiate between the various drug release mechanisms, also considering the nature and geometry of the drug delivery system, as shown in Table 4 [64,65].

Table 4. Interpretation of diffusional release mechanisms considering the values of diffusional exponent n and the geometry of the delivery systems.

Diffusional Exponent, n			Drug Release Mechanism	Ref.
Thin film	Cylinder	Sphere		
0.5	0.45	0.43	Fickian diffusion	[63–65]
0.5 < n < 1	0.45 < n < 0.89	0.43 < n < 0.85	Anomalous (non-Fickian) transport	
1	0.89	0.85	Case-II transport	

According to Table 4, for n values equal to 0.5, Fickian diffusion release is valid, while higher values of n between 0.5 and 1 suggest a non-Fickian behavior which also takes into consideration the erosion of the polymer chain. Values of n equal to 1 correspond to zero order kinetics release, when drug release is independent of time [63–65]. Generally, Equation (1) should be applicable to the first 60% of the cumulative drug release fraction (R < 60%) [63–65].

Table 5 presents the values of the calculated parameters for the doped PPy coatings electrochemically synthesized from ILM-ACN based electrolytes and various Indo concentrations, on IB and ND substrates, respectively.

Table 5. Results of curve fitting using Equation (1) of indomethacin release data from different PPy-Indo coatings electrosynthesized on IB and ND alloy substrates using ILM-ACN based electrolyte containing 0.5 M Py and various Indo concentrations.

System	Parameters		
	n	k/h^{-1}	r^2
IB-PPy-0.0125 M Indo	0.493	5.328	0.9638
IB-PPy-0.0175 M Indo	0.522	5.243	0.9688
IB-PPy-0.025 M Indo	0.523	7.228	0.9943
IB-PPy-0.05 M Indo	0.623	6.309	0.9830
ND-PPy-0.0125 M Indo	0.399	5.731	0.9821
ND-PPy-0.0175 M Indo	0.432	5.006	0.9583
ND-PPy-0.025 M Indo	0.446	5.253	0.9754
ND-PPy-0.05 M Indo	0.441	5.814	0.9918

The correlation coefficients (r^2) determined during the fit of the Korsmeyer–Peppas model to the experimental release data for all PPy-Indo coatings suggest that the indomethacin release can be described using this model. The diffusional exponent (n) ranged between 0.493 and 0.623 for the PPy-Indo coatings electrosynthesized on the IB alloy substrate, indicating that the diffusion of the drug out of the polymer layer is a mechanism governing the release. In the case of PPy-Indo coatings electrosynthesized on the ND alloy substrate, the n values were calculated to be in the range of 0.399–0.441, suggesting the indomethacin release controlled by a lower diffusivity, possibly related to the slightly more compact morphology of the layer [65].

The kinetic constant (k) shows relatively high values, suggesting a fast release of the drug from the PPy coatings, more pronounced in the case of those electrosynthesized on the IB substrate.

4. Conclusions

Polypyrrole and polypyrrole-indomethacin coatings have been successfully synthesized on different types of NiCr alloy substrates (IB and ND) widely used in dentistry, involving electrochemical polymerization of pyrrole using eutectic mixtures of choline chloride and malonic acid. This appears to be the first report related to the electropolymerization of pyrrole on NiCr alloy metallic substrates involving DESs. This type of electrolyte allowed an enhanced dissolution of indomethacin as compared to aqueous ones.

Electrochemical polymerization rates have been estimated from the gradient of the charge–time plots, ranging between 2.16 and 3.54 mC s^{-1} (1.44–2.36 mC cm^{-2} s^{-1}) and 2.0 and 4.83 mC s^{-1} (1.3–3.22 mC cm^{-2} s^{-1}) for the IB and ND substrates, respectively, with no loss of the conductivity of the deposited polymer. SEM micrographs of the polypyrrole-indomethacin coatings evidenced a rather granular surface morphology and no insoluble precipitates of the drug molecules were detected on the surface. The recorded FTIR spectra confirmed the presence of indomethacin in the polypyrrole structure. The SBF contact angle measurements suggested that the doping of the polymer with the drug molecule facilitates an improvement of the overall hydrophilic characteristics. The PPy-Indo layers were found to provide better corrosion protection compared to the pure PPy ones in SBF environment, mainly due to the inhibition of the anodic reaction.

Indomethacin release tests showed that the PPy-Indo coatings may deliver the drug molecule for longer periods of at least 17 days. The maximum released amount was found to be around 99.6% suggesting that the synthesized polypyrrole coating layers acted as an active reservoir for indomethacin.

The release profiles suggested that the diffusion of the drug out of the polymer layer is the mechanism governing the release.

The obtained results showed some of the advantages of the use of DESs, providing both an easier route for the electrochemical synthesis of doped conducting polymers on commonly used metallic substrates and an improved solubility of poor soluble drugs as is the case with indomethacin. The procedure would contribute to the growth of promising films suitable to be used as biocompatible materials. The electrochemical behavior in complex DES based formulations will be further investigated for a deeper understanding of the polymerization mechanism occurring in these electrolytic media.

Author Contributions: Conceptualization, F.G. and L.A.; methodology, F.G.; validation, F.G. and L.A.; formal analysis, M.-S.C. and A.-G.P.; investigation, M.-S.C. and A.-G.P.; writing—original draft preparation, F.G.; writing—review and editing, L.A.; supervision, L.A. All authors have read and agreed to the published version of the manuscript.

Funding: This research was partially funded by Romanian Ministry of Education and by Executive Agency for Higher Education, Research, Development and Innovation Funding, under NOVTINALBEST project 38/2016, M Era Net Program.

Conflicts of Interest: The authors declare no conflict of interest.

References

1. Wataha, J.C. Biocompatibility of dental casting alloys: A review. *J. Prosthet. Dent.* **2000**, *83*, 223–234. [CrossRef]
2. Saji, V.S.; Choe, H.C. Electrochemical behavior of Co-Cr and Ni-Cr dental cast alloys. *Trans. Nonferrous Met. Soc. China* **2009**, *19*, 785–790. [CrossRef]
3. Wataha, J.C.; O'Dell, N.L.; Singh, B.B.; Ghazi, M.; Whitford, G.M.; Lockwood, P.E. Relating nickel induced tissue inflammation to nickel release in vivo. *J. Biomed. Mater. Res.* **2001**, *58*, 537−544.
4. Schmalz, G.; Garhammer, P. Biological interactions of dental cast alloys with oral tissues. *J. Dent. Mater.* **2002**, *18*, 396−406. [CrossRef]
5. Reclaru, L.; Ziegenhagen, R.; Unger, R.E.; Eschler, P.Y.; Constantin, F. New generation super alloy candidates for medical applications: Corrosion behavior, cation release and biological evaluation. *Mater. Sci. Eng. C* **2014**, *45*, 411–420. [CrossRef]
6. Romonti, D.; Milosev, I.; Demetrescu, I. Effect of sodium fluoride on the stability of dental alloys in artificial saliva. *Rev. Chim. (Bucharest)* **2016**, *67*, 1097–1103.
7. Aljohani, T.; Hayden, B.; Anastasopoulos, A. The high throughput electrochemical screening of the corrosion resistance of Ni–Cr thin film alloys. *Electrochim. Acta* **2012**, *76*, 389–393. [CrossRef]
8. Reclaru, L.; Unger, R.E.; Kirkpatrick, C.J.; Susz, C.; Eschler, P.-Y.; Zuercher, M.-H.; Antoniac, I.; Lüthy, H. Ni–Cr based dental alloys; Ni release, corrosion and biological evaluation. *Mater. Sci. Eng. C* **2012**, *32*, 1452–1460. [CrossRef]
9. Duffo, G.; Farina, S. Corrosion behaviour of a dental alloy in some beverages and drinks. *Mat. Chem. Phys.* **2009**, *115*, 235–238. [CrossRef]
10. Manam, N.S.; Harun, W.S.W.; Shri, D.N.A.; Ghani, S.A.C.; Kurniawan, T.; Ismail, M.H.; Ibrahim, M.H.I. Study of corrosion in biocompatible metals for implants. *J. Alloys Compd.* **2017**, *701*, 698–715. [CrossRef]
11. Arrieta-González, C.D.; Porcayo-Calderon, J.; Salinas-Bravo, V.M.; Chacon-Nava, J.G.; Martinez-Villafañe, A.; Gonzalez-Rodriguez, J.G. Corrosion behavior of Ni-Cr based coatings in simulated human body fluid environment. *Int. J. Electrochem. Sci.* **2011**, *6*, 3644–3655.
12. Golgovici, F.; Ionascu, F.G. Electrochemical behavior of NiCr based alloys in human and artificial saliva. *UPB Sci. Bull. B* **2017**, *79*, 157–166.
13. Covaciu Romonti, D.; Voicu, G.; Prodana, M. Electrochemical behavior of coated and uncoated nonprecious CoCr and NiCr alloys in artificial and natural saliva. *Int. J. Electrochem. Sci.* **2015**, *10*, 6935–6945.
14. Guimard, N.K.; Gomez, N.; Schmidt, C.E. Conducting polymers in biomedical engineering. *Prog. Polym. Sci.* **2007**, *32*, 876–921. [CrossRef]
15. Alshammary, B.; Walsh, F.C.; Herrasti, P.; Ponce de Leon, C. Electrodeposited conductive polymers for controlled drug release: Polypyrrole. *J. Solid State Electrochem.* **2016**, *20*, 839–859. [CrossRef]

16. Antoniac, I.; Albu, M.; Sinescu, C.; Miculescu, M. Corrosion behavior of TiSiN coatings deposited on Ni-Cr alloy in artificial saliva with and without fluoride. *Key Eng. Mater.* **2015**, *638*, 47–53.
17. Sella, C.; Martin, J.C.; Lecoeurm, J.; Bellier, J.P.; Davidas, J.P. Corrosion and protection of surgical and dental metallic implants. In *Biocompatibility of Co-Cr-Ni Alloys*; Hildebrand, H.F., Champy, M., Eds.; NATO ASI series. Series A, Life sciences; Plenum Press: New York, NY, USA, 1988; Volume 158, pp. 349–362.
18. Shah, S.A.A.; Firlak, M.; Berrow, S.R.; Halcovitch, N.R.; Baldok, S.J.; Yousafzai, B.M.; Hathout, R.M.; Hardy, J.G. Electrochemically enhanced drug delivery using polypyrrole films. *Materials* **2018**, *11*, 1123. [CrossRef]
19. Kohrs, N.J.; Liyanage, T.; Venkatesan, N.; Najarzadeh, A.; Puleo, D.A. Drug delivery systems and controlled release. In *Encyclopedia of Biomedical Engineering*, 1st ed.; Narayan, R., Ed.; Elsevier: Amsterdam, The Netherlands, 2018.
20. Egorova, K.S.; Gordeev, E.G.; Ananikov, V.P. Biological activity of ionic liquids and their application in pharmaceutics and medicine. *Chem. Rev.* **2017**, *117*, 7132–7189. [CrossRef]
21. Caparica, R.; Julio, A.; Baby, A.R.; Machado Araujo, M.E.; Fernandes, A.S.; Costa, J.G.; Santos de Almeida, T. Choline-amino acid ionic liquids as green functional excipients to enhance drug solubility. *Pharmaceutics* **2018**, *10*, 288. [CrossRef]
22. Beyersdorff, T.; Schubert, T.J.S.; Wetz-Biermann, U.; Pitner, W.; Abbott, A.P.; McKenzie, K.J.; Ryder, K.S. Synthesis of ionic liquids. In *Electrodeposition from Ionic Liquids*, 2nd ed.; Endres, F., Abbott, A., MacFarlane, D., Eds.; Wiley-VCH KGaA: Weinheim, Germany, 2017; pp. 17–54.
23. Johnson, K.E. What's an ionic liquid? *Interface* **2007**, *16*, 38–41.
24. Sidat, Z.; Marimuthu, T.; Kumar, P.; du Toit, L.C.; Kondiah, P.P.D.; Choonara, Y.E.; Pillay, V. Ionic liquids as potential and synergistic permeation enhancers for transdermal drug delivery. *Pharmaceutics* **2019**, *11*, 96. [CrossRef] [PubMed]
25. Santos de Almeida, T.; Júlio, A.; Saraiva, N.; Fernandes, A.S.; Araújo, M.E.M.; Baby, A.R.; Rosado, C.; Mota, J.P. Choline-versus imidazole-based ionic liquids as functional ingredients in topical delivery systems: Cytotoxicity, solubility, and skin permeation studies. *Drug Dev. Ind. Pharm.* **2017**, *43*, 1858–1865. [CrossRef] [PubMed]
26. Pedro, S.N.; Freire, M.G.; Freire, C.S.R.; Silvestre, A.J.D. Deep eutectic solvents comprising active pharmaceutical ingredients in the development of drug delivery systems. *Expert Opin. Drug Del.* **2019**, *16*, 497–506. [CrossRef] [PubMed]
27. Li, Z.; Lee, P.I. Investigation on drug solubility enhancement using deep eutectic solvents and their derivatives. *Int. J. Pharm.* **2016**, *505*, 283–288. [CrossRef] [PubMed]
28. Abbott, A.P.; Capper, G.; Davies, D.L.; Munro, H.; Rasheed, R.; Tambyrajah, V. Preparation of novel, moisture-stable, Lewis-acidic ionic liquids containing quaternary ammonium salts with functional side chains. *Chem. Commun.* **2001**, *19*, 2010–2011. [CrossRef] [PubMed]
29. Abbott, A.P.; Capper, G.; Davies, D.L.; Rasheed, R.K.; Tambyrajah, V. Novel solvent properties of choline chloride/urea mixtures. *Chem. Commun.* **2003**, *1*, 70–71. [CrossRef]
30. Abbott, A.P.; Boothby, D.; Capper, G.; Davies, D.L.; Rasheed, R.K. Deep eutectic solvents formed between choline chloride and carboxylic acids: Versatile alternatives to ionic liquids. *J. Am. Chem. Soc.* **2004**, *126*, 9142–9147. [CrossRef]
31. Mirgorodskaya, A.; Kushnazarova, R.; Nikitina, A.; Semina, I.; Nizameev, I.; Kadirov, M.; Khutoryanskiy, V.; Zakharova, L.; Sinyashin, O. Polyelectrolyte nanocontainers: Controlled binding and release of indomethacin. *J. Mol. Liq.* **2018**, *272*, 982–989. [CrossRef]
32. Genari, B.; Leitune, V.C.B.; Jornada, D.S.; Camassola, M.; Pohlmann, A.R.; Guterres, S.S.; Samuel, S.M.W.; Collares, F.M. Effect of indomethacin-loaded nanocapsules incorporation in a dentin adhesive resin. *Clin. Oral Investig.* **2017**, *21*, 437–446. [CrossRef]
33. Comer, J.; Judge, S.; Matthews, D.; Towes, L.; Falcone, B.; Goodman, J.; Dearden, J. The intrinsic aqueous solubility of indomethacin. *ADMET DMPK* **2014**, *2*, 18–32. [CrossRef]
34. Patel, A.; Cholkar, K.; Agrahari, V.; Mitra, A.K. Ocular drug delivery systems: An overview. *World J. Pharmacol.* **2013**, *2*, 47–64. [CrossRef] [PubMed]
35. Ruidiaz, M.A.; Delgado, D.R.; Mora, C.P.; Yurquina, A.; Martínez, F. Estimation of the indomethacin solubility in ethanol + water mixtures by the extended Hildebrand solubility approach. *Rev. Colomb. Cienc. Quím. Farm.* **2010**, *39*, 79–95.

36. Mokhtarpour, M.; Shekaari, H.; Martinez, F.; Zafarani-Moattar, M.T. Effect of tetrabutylammonium bromide-based deep eutectic solvents on the aqueous solubility of indomethacin at various temperatures: Measurement, modeling, and prediction with three-dimensional Hansen solubility parameters. *AAPS PharmSciTech* **2019**, *20*, 204. [CrossRef]
37. Skopek, M.A.; Mohamoud, M.A.; Ryder, K.S.; Hillman, A.R. Nanogravimetric observation of unexpected ion exchange characteristics for polypyrrole film p-doping in a deep eutectic solvent. *Chem. Commun.* **2009**, *8*, 935–937. [CrossRef] [PubMed]
38. Pigani, L.; Tezi, F.; Dossi, N.; Toniolo, R. Electropolymerisation and electrochemical behavior of polypyrrole in deep eutectic solvents. In *An EQCM Study, Book of Abstracts of GS 2015: Sensori e Biosensori: Stato Dell'arte e Nuove Prospettive*; Parma, Italy, 15–17 June 2015; p. 56 (P-12). Available online: http://www.gs2015.unipr.it/book_of_abstracts2015.pdf (accessed on 5 June 2020).
39. Golgovici, F.; Anicai, L.; Florea, A.; Visan, T. Electrochemical synthesis of conducting polymers involving deep eutectic solvents. *Curr. Nanosci.* **2020**, *16*, 478–494. [CrossRef]
40. Anicai, L.; Cojocaru, A.; Florea, A.; Visan, T. Electrochemical investigation of silver/silver ion couple reversibility in choline chloride-urea based ionic liquid. *Stud. Univ. Babes-Bolyai Chem.* **2008**, *53*, 119–133.
41. Kokubo, T.; Takadama, H. How useful is SBF in predicting in vivo bone bioactivity? *Biomaterials* **2006**, *27*, 2907–2915. [CrossRef]
42. Mares Badea, M.L.; Cojocaru, A.; Anicai, L. Electrode processes in ionic liquid solvents as mixtures of choline chloride with urea, ethylene glycol or malonic acid. *UPB Sci. Bull. Ser. B* **2014**, *76*, 21–32.
43. Garfias-García, E.; Romero-Romo, M.; Ramírez-Silva, M.T.; Morales, J.; Palomar-Pardavé, M. Electrochemical nucleation of polypyrrole onto different substrates. *Int. J. Electrochem. Sci.* **2010**, *5*, 763–773.
44. Pringle, J.M.; Efthimiadis, J.; Howlett, P.C.; Efthimiadis, J.; MacFarlane, D.R.; Chaplin, A.B.; Hall, S.B.; Officer, D.L.; Wallace, G.G.; Forsyth, M. Electrochemical synthesis of polypyrrole in ionic liquids. *Polymer* **2004**, *45*, 1447–1453. [CrossRef]
45. Castagno, K.R.L.; Dalmoro, V.; Azambuja, D.S. Characterization and corrosion of polypyrrole/sodium dodecylbenzene sulfonate electropolymerised on aluminum alloy 1100. *Mater. Chem. Phys.* **2011**, *130*, 721–726. [CrossRef]
46. Ryan, E.; Breslin, C. The incorporation of drug molecules with poor water solubility into polypyrrole as dopants: Indomethacin and sulindac. *Electrochim. Acta* **2019**, *296*, 848–855. [CrossRef]
47. Flamini, D.O.; Valle, M.I.; Sandoval, M.J.; Massheimer, V.L.; Saidman, S.B. Electrodeposition study of polypyrrole-heparin and polypyrrole-salicylate coatings on Nitinol. *Mater. Chem. Phys.* **2018**, *209*, 76–85. [CrossRef]
48. Anderson, B.D. Predicting solubility/miscibility in amorphous dispersions: It is time to move beyond regular solution theories. *J. Pharm. Sci.* **2018**, *107*, 24–33. [CrossRef]
49. Xiang, T.-X.; Anderson, B.D. Molecular dynamics simulation of amorphous indomethacin. *Mol. Pharm.* **2013**, *10*, 102–114. [CrossRef]
50. Ewing, A.; Clarke, G.; Kazarian, S. Stability of indomethacin with relevance to the release from amorphous solid dispersions studied with ATR-FTIR spectroscopic imaging. *Eur. J. Pharm. Sci.* **2014**, *60*, 64–71. [CrossRef]
51. Jain, K.; Darwhekar, G.; Solanki, S.S.; Sharma, R. Osmotically regulated asymmetric capsular system for sustained delivery of indomethacin. *J. Pharm. Investig.* **2012**, *43*, 27–35. [CrossRef]
52. Yussuf, A.; Al-Saleh, M.; Al-Enezi, S.; Abraham, G. Synthesis and characterization of conductive polypyrrole: The influence of the oxidants and monomer on the electrical, thermal, and morphological properties. *Int. J. Polym. Sci.* **2018**, 4191747. [CrossRef]
53. Matsumoto, Y.; Honma, K. NH stretching vibrations of pyrrole clusters studied by infrared cavity ringdown spectroscopy. *J. Chem. Phys.* **2007**, *127*, 184310. [CrossRef]
54. Ibrahim, I.M.; Yunus, S.; Hashim, M.A. Relative performance of isopropylamine, pyrrole and pyridine as corrosion inhibitors for carbon steels in saline water at mildly elevated temperatures. *Int. J. Eng. Res.* **2013**, *4*, 1–12.
55. Omastova, M.; Trchova, M.; Kovarova, J.; Stejskal, J. Synthesis and structural study of polypyrroles prepared in the presence of surfactants. *Synth. Met.* **2003**, *138*, 447–455. [CrossRef]

56. Dong, H.; Li, Q.; Tan, C.; Bai, N.; Cai, P. Bi-directional controlled release of ibuprofen and Mg^{2+} from magnesium alloys coated by multifunctional composite. *Mater. Sci. Eng. C* **2016**, *68*, 512–518. [CrossRef] [PubMed]
57. Cho, Y.; Borgens, R.B. Biotin-doped porous polypyrrole films for electrically controlled nanoparticle release. *Langmuir* **2011**, *27*, 6316–6322. [CrossRef] [PubMed]
58. Bard, A.J. *Electrochemical Methods—Fundamentals and Applications*; John Wiley & Sons: New York, NY, USA, 2000.
59. Anicai, L.; Florea, A.; Buda, M.; Visan, T. Polypyrrole films doped with phosphomolybdate anions on Al surfaces-Formation and corrosion protection characterisation. *Z. Phys. Chem.* **2013**, *227*, 1121–1141. [CrossRef]
60. Stern, M.; Geary, A.L. Electrochemical polarization: I A theoretical analysis of the shape of polarization curves. *J. Electrochem. Soc.* **1957**, *104*, 56–63. [CrossRef]
61. Aroso, I.M.; Craveiro, R.; Rocha, A.; Dionisio, M.; Barreiros, S.; Reis, R.L.; Paiva, A.; Duarte, A.R.C. Design of controlled release systems for THEDES—Therapeutic deep eutectic solvents, using supercritical fluid technology. *Int. J. Pharm.* **2015**, *492*, 73–79. [CrossRef]
62. Siepmann, J.; Siepmann, F. Modelling of diffusion controlled drug delivery. *J. Control. Release* **2012**, *161*, 351–362. [CrossRef]
63. Costa, P.; Lobo, J.M.S. Modeling and comparison of dissolution profiles. *Eur. J. Phar. Sci.* **2001**, *13*, 123–133. [CrossRef]
64. Ritger, P.L.; Peppas, N.A. A simple equation for description of solute release. I. Fickian and non-Fickian release from non-sweliable devices in the form of slabs, spheres, cylinders or discs. *J. Control. Release* **1987**, *5*, 23–36. [CrossRef]
65. Korsmeyer, R.; Gurny, R.; Doelker, E.; Peppas, N. Mechanisms of solute release from porous hydrophilic polymers. *Int. J. Pharm.* **1983**, *15*, 25–35. [CrossRef]